Analysis and Correction of LEO Satellite Propagation Errors with Application to Navigation

Samer Hayek, Joe Saroufim, and Zaher M. Kassas
The Ohio State University

BIOGRAPHY

Samer Hayek is a Ph.D student in the Department of Electrical and Computer Engineering at The Ohio State University and a member of the Autonomous Systems Perception, Intelligence, and Navigation (ASPIN) Laboratory. He received a B.E. in Mechanical Engineering from the Lebanese American University. His current research interests include low Earth orbit satellites, autonomous vehicles, sensor fusion, and simultaneous localization and mapping.

Joe Saroufim is a Ph.D student in the Department of Electrical and Computer Engineering at The Ohio State University and a member of the ASPIN Laboratory. He received a B.E. in Mechanical Engineering from the Lebanese American University. His current research interests include low Earth orbit satellites, situational awareness, autonomous vehicles, and sensor fusion.

Zaher (Zak) M. Kassas is the TRC Endowed Chair in Intelligent Transportation Systems and a professor at The Ohio State University. He is the Director of the ASPIN Laboratory. He is also Director of the U.S. Department of Transportation Center: CARMEN (Center for Automated Vehicle Research with Multimodal AssurEd Navigation), focusing on navigation resiliency and security of highly automated transportation systems. He received a B.E. with Honors in Electrical Engineering from the Lebanese American University, an M.S. in Electrical and Computer Engineering from The Ohio State University, and an M.S.E. in Aerospace Engineering and a Ph.D. in Electrical and Computer Engineering from The University of Texas at Austin. He is a recipient of the National Science Foundation (NSF) CAREER award, Office of Naval Research (ONR) Young Investigator Program (YIP) award, Air Force Office of Scientific Research (AFOSR) YIP award, IEEE Walter Fried Award, IEEE Harry Rowe Mimno Award, Institute of Navigation (ION) Samuel Burka Award, and ION Col. Thomas Thurlow Award. He is a Fellow of the IEEE, a Fellow of the ION, and a Distinguished Lecturer of the IEEE Aerospace and Electronic Systems Society and the IEEE Intelligent Transportations Systems Society. His research interests include cyber-physical systems, navigation systems, low Earth orbit satellites, cognitive sensing, and intelligent transportation systems.

ABSTRACT

The propagation error dynamics of low Earth orbit (LEO) space vehicles (SVs) are analyzed and modeled, leading to an approach to correct these errors. The approach maps a propagation error in the SV's argument of latitude orbital element to an error in the SV's position and velocity states, resolved in the SV's body frame of reference. The effect of an ephemeris epoch time adjustment on LEO SV orbit errors is examined using orbital dynamics. Implementing the epoch time adjustment is demonstrated to significantly decrease open-loop simplified general perturbations (SGP4)-propagated ephemeris errors with (i) real transmitted orbit data from an Orbcomm LEO SV and (ii) SpaceX published accurate orbit data describing four Starlink LEO SVs. Finally, experimental results are presented, evaluating opportunistic unmanned aerial vehicle (UAV) navigation with carrier phase measurements from 2 Orbcomm LEO SVs. The UAV traversed a trajectory of 780 m in 90 seconds. Global navigation satellite system (GNSS) signals were only available to the UAV during the first 30 seconds of the flight duration, during which the proposed ephemeris correction approach was performed, after which GNSS signals were cut off for the remaining 60 seconds, during which the UAV navigated with signals from the 2 LEO SVs. It is shown that using open-loop SGP4-propagated ephemerides for the LEO SVs yields a three-dimensional (3D) UAV position root-mean squared-error (RMSE) of 75.69 m, while incorporating the corrected ephemerides resulted in a position RMSE of 12.28 m.

I. INTRODUCTION

The advent of recent and upcoming low Earth orbit (LEO) satellite megaconstellations is shaping a new era of satellite-based navigation. LEO-based communication has been offered over the past couple of decades by LEO constellations such as Orbcomm, Iridium, and Globalstar; each of which composed of tens of LEO space vehicles (SVs). However, the birth of LEO megaconstellations such as Starlink, OneWeb, and Kuiper; which are aggregately planning to launch tens of thousands of LEO SVs is promising to revolutionize several domains, bringing unprecedented high-resolution images; remote sensing; and global, high-availability, high-bandwidth, and low-latency Internet (Osoro and Oughton, 2021). Recently, the growing interest

Preprint of the 2024 ION GNSS+ Conference
Baltimore, Maryland, September 16–20, 2024

in utilizing LEO SVs for navigation purposes has been the subject of several theoretical and experimental studies (Morales et al., 2018; Jardak and Jault, 2022; Singh et al., 2022; Prol et al., 2022; Kassas et al., 2023; Shi et al., 2023; Yang et al., 2023; Khalife and Kassas, 2023; Farhangian and Landry, 2023; Jiang et al., 2023; Zhao et al., 2023; Liu et al., 2024; Prol et al., 2024; Kang et al., 2024).

This growing research effort towards LEO satellite-based positioning, navigation, and timing (PNT) is mainly due to their desirable attributes (Stock et al., 2024): (i) abundance and geometric diversity, (ii) high received signal power, (iii) high orbital velocity, and (iv) spectral diversity. These inherent qualities present LEO-PNT systems as a complement or even an alternative to classic GNSS systems that reside in the medium Earth orbit (MEO), and whose signals are vulnerable to attenuation and interference (Ioannides et al., 2016; Hegarty et al., 2020; Burbank et al., 2024). While some studies proposed to design navigation-dedicated LEO satellite constellation signals (Reid et al., 2020; Celikbilek et al., 2022; Egea-Roca et al., 2022; Ferre et al., 2022; Ries et al., 2023; Menzione and Paonni, 2023; Yan et al., 2023), other research proposed to exploit LEO SV signals for navigation in an opportunistic fashion (Kassas et al., 2019; Zhao et al., 2022; Singh et al., 2022; Kozhaya et al., 2023; Stock et al., 2023; Saroufim et al., 2023; Grayver et al., 2024; Kassas et al., 2024).

Opportunistic navigation with LEO SVs considers minimal or imperfect knowledge about the SV signals or ephemerides at the user (receiver) end. Recent designs of specialized receivers leveraged the periodicity in LEO SV signals (Landry et al., 2019; Khalife and Kassas, 2019; Huang et al., 2022; Liang et al., 2024) or adopted blind frameworks (cognitive receivers) (Khalife et al., 2021, 2022; Kozhaya and Kassas, 2023; Shahcheraghi and Kassas, 2024) to estimate key signal parameters and consequently generate navigation observables. In contrast to GNSS SVs that transmit ephemeris data and clock corrections in their navigation message, most LEO SVs are operated by private companies that do not publicly share information about the SV's position, velocity, and time. Therefore, the user must ensure continuous or intermittent access to reliable LEO SV ephemerides (Ardito et al., 2019) or implement a sufficiently accurate orbit initialization and propagation scheme in order to employ their navigation observables in a positioning or navigation solution (Shuster, 2017).

A common source of LEO SV ephemerides data is the North American Aerospace Defense Command (NORAD) published two-line element (TLE) files. TLE files are updated a few times a day and consist of designation, epoch time, and atmospheric drag parameter data, in addition to the SV Keplerian orbital elements: inclination, right ascension of ascending node, eccentricity, argument of perigee, mean anomaly, and mean motion (Kelso, 2022). The simplified general perturbation 4 (SGP4) software (Vallado and Crawford, 2008) is compatible with TLE files that are used to initialize the propagator. The reasons for inaccuracies resulting from the TLE-initialized SGP4-propagation scheme are two fold. First, TLE data describing LEO SV orbits suffer from inherent errors (Coffee et al., 2013; Riesing, 2015). The calculation of Keplerian elements from the SV's position and velocity vectors may cause practical and numerical issues, specifically in the presence of singular orbital elements (Montenbruck and Gill, 2000). Second, similarly to most orbit propagators, SGP4 involves dynamical models for the various forces acting on an SV, including gravitational forces, atmospheric drag, and solar radiation pressure. Nevertheless, orbit propagation through SGP4 has been shown to exhibit errors concentrated along the SV's direction of motion (Kelso, 2007). Specifically, it was found that SGP4 propagation induces a linearly increasing error in the SV's argument of latitude orbital element (Easthope, 2015). Previous work studied the recursive estimation of the argument-of-latitude to mitigate the large ephemeris errors inherited from TLE-initialized SGP4 orbit propagation (Hayek et al., 2023, 2024).

This paper focuses on the analysis and modeling of LEO SV orbit propagation errors to meet accurate PNT requirements by refining publicly available ephemeris data. This paper presents the following contributions. First, analytical models for the error propagation from the argument of latitude orbital element to the SV body frame position and velocity states are derived. Second, the effect of an ephemeris epoch time adjustment on the orbit errors is analyzed by examining the underlying dynamics. Implementing the epoch time adjustment is demonstrated to significantly decrease open-loop SGP4-propagated ephemeris errors with (i) real transmitted orbit data from an Orbcomm LEO SV and (ii) SpaceX published accurate orbit data describing four Starlink LEO SVs. Finally, experimental results are presented, evaluating opportunistic unmanned aerial vehicle (UAV) navigation with carrier phase measurements from 2 Orbcomm LEO SVs. The UAV traversed a trajectory of 780 m in 90 seconds. Global navigation satellite system (GNSS) signals were only available to the UAV during the first 30 seconds of the flight duration, during which the proposed ephemeris correction approach was performed, after which GNSS signals were cut off for the remaining 60 seconds, during which the UAV navigated with signals from the 2 LEO SVs. It is shown that using open-loop SGP4-propagated ephemerides for the LEO SVs yields a three-dimensional (3D) UAV position root-mean squared-error (RMSE) of 75.69 m, while incorporating the corrected ephemerides resulted in a position RMSE of 12.28 m.

The rest of the paper is organized as follows. Section II describes the modeling and analysis of LEO SV propagation errors and the effect of epoch time adjustment. Section III presents experimental results of UAV opportunistic navigation using corrected ephemerides sets. Section IV gives concluding remarks.

II. MODEL DESCRIPTION

This section presents analytical models for LEO SV position and velocity propagation errors and the effect of an ephemeris epoch time adjustment on the error dynamics.

1. Satellite Orbital Elements

The SV's dynamic state can be described in terms of the six classical orbital elements: angular momentum magnitude h, eccentricity e, inclination i, right ascension of the ascending node Ω, argument of perigee ω, and the true anomaly ν. The SV's motion is governed by the time derivatives of the the orbital elements that are described in Gauss' planetary equations (Curtis, 2019) as:

$$\begin{aligned}
\frac{de}{dt} &= \frac{3J_2\mu R_\text{e}^2}{2hr_\text{s}^3}\left\{\frac{h^2}{\mu r_\text{s}}\sin\nu(3\sin^2 i\sin^2 u-1)-\sin(2u)\sin^2 i[(3+e\cos\nu)\cos\nu+e]\right\}\\
\frac{d\omega}{dt} &= \frac{3J_2\mu R_\text{e}^2}{2ehr_\text{s}^3}\left[\frac{h^2}{\mu r_\text{s}}\cos\nu(1-3\sin^2 i\sin^2 u)-(2+e\cos\nu)\sin(2u)\sin^2 i\sin\nu+2e\cos^2 i\sin^2 u\right]\\
\frac{d\nu}{dt} &= \frac{h}{r_\text{s}^2}+\frac{3J_2\mu R_\text{e}^2}{2ehr_\text{s}^3}\left[\frac{h^2}{\mu r_\text{s}}\cos\nu(3\sin^2 i\sin^2 u-1)+(2+e\cos\nu)\sin(2u)\sin^2 i\sin\nu\right]\\
\frac{du}{dt} &= \frac{h}{r_\text{s}^2}+\frac{3J_2\mu R_E^2}{2ehr_\text{s}^3}(2e\cos^2 i\sin^2 u),
\end{aligned} \tag{1}$$

where μ is the Earth's standard gravitational parameter, R_e is the mean radius of the Earth, J_2 is the second zonal harmonic coefficient, $r_\text{s} \triangleq \|\boldsymbol{r}_\text{s}\|$, and $h \triangleq \|\boldsymbol{h}\|$ is the magnitude of the angular momentum vector $\boldsymbol{h} \triangleq \boldsymbol{r}_\text{s} \times \dot{\boldsymbol{r}}_\text{s}$. Fig. 1 shows the instantaneous time derivatives of the orbital elements over a 6-hour duration for Starlink ID 48010, that has an orbital period of about 95 minutes.

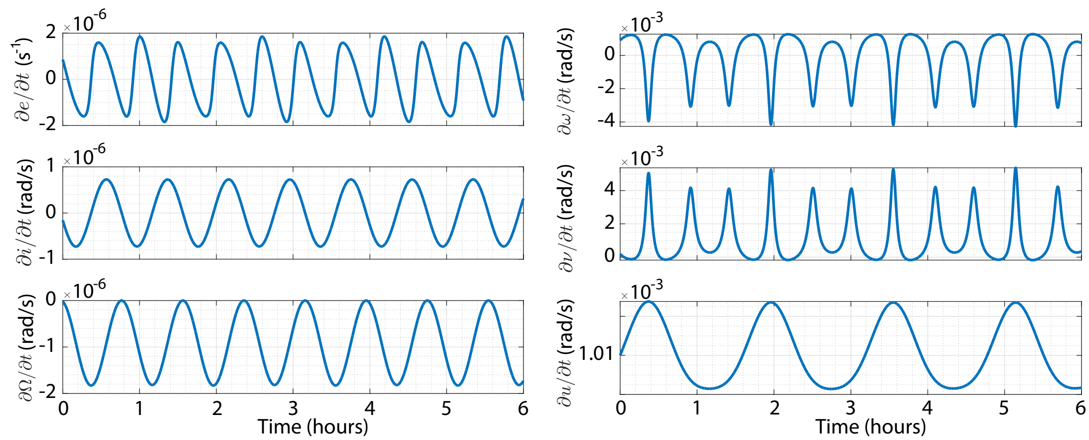

Figure 1: Time derivatives of the orbital elements for Starlink 48010.

The argument of latitude $u \triangleq \omega+\nu$ is the angle from the line of nodes, i.e., the intersection of the orbital and equatorial planes, to the SV position vector. It can be seen in Fig. 1 that the rates of the argument of perigee, true anomaly, and the argument of latitude are 3 orders of magnitude higher than the rates of the eccentricity, inclination, and right ascension, indicating that most of the SV dynamics are concentrated in the argument of latitude element.

2. Satellite Propagation Error Dynamics

The SV's position and velocity vectors in the Earth-centered inertial (ECI) frame {i} can be written in terms of the orbital elements (Montenbruck and Gill, 2000) as

$${}^i\boldsymbol{r}_\text{s} = r_\text{s}\begin{bmatrix}\cos u\cos\Omega-\sin u\cos i\sin\Omega\\ \cos u\sin\Omega+\sin u\cos i\cos\Omega\\ \sin u\sin i\end{bmatrix} \quad\text{and}\quad {}^i\dot{\boldsymbol{r}}_\text{s} = \frac{\mu}{h}\begin{bmatrix}-\cos\Omega(\sin u+e\sin\omega)-\sin\Omega\cos i(\cos u+e\cos\omega)\\ -\sin\Omega(\sin u+e\sin\omega)+\cos\Omega\cos i(\cos u+e\cos\omega)\\ \sin i(\cos u+e\cos\omega)\end{bmatrix}. \tag{2}$$

Since most of the ephemeris prediction error is concentrated in the argument-of-latitude element, the prediction errors for r, i, and Ω will be neglected; thus, the predicted SV position and velocity are written as

$$ {}^{i}\boldsymbol{r}'_{\mathrm{s}} \approx r_{\mathrm{s}} \begin{bmatrix} \cos u' \cos\Omega - \sin u' \cos i \sin\Omega \\ \cos u' \sin\Omega + \sin u' \cos i \cos\Omega \\ \sin u' \sin i \end{bmatrix} \quad \text{and} \quad {}^{i}\dot{\boldsymbol{r}}'_{\mathrm{s}} \approx \frac{\mu}{h} \begin{bmatrix} -\cos\Omega(\sin u' + e\sin\omega) - \sin\Omega\cos i(\cos u' + e\cos\omega) \\ -\sin\Omega(\sin u' + e\sin\omega) + \cos\Omega\cos i(\cos u' + e\cos\omega) \\ \sin i(\cos u' + e\cos\omega) \end{bmatrix}, \tag{3} $$

where u' represents the predicted argument of latitude. The SV position and velocity errors are defined as

$$ \tilde{\boldsymbol{r}}_{\mathrm{s}} \triangleq \boldsymbol{r}_{\mathrm{s}} - \boldsymbol{r}'_{\mathrm{s}} \quad \text{and} \quad \tilde{\dot{\boldsymbol{r}}}_{\mathrm{s}} \triangleq \dot{\boldsymbol{r}}_{\mathrm{s}} - \dot{\boldsymbol{r}}'_{\mathrm{s}}. $$

The ephemeris errors of the predicted orbit in the ECI frame $\{i\}$ can be represented in the SV's body frame $\{b\}$, namely the RSW frame, as

$$ {}^{b}\tilde{\boldsymbol{r}}_{\mathrm{s}} = \mathbf{R}_i^b \, {}^{i}\tilde{\boldsymbol{r}}_{\mathrm{s}} \qquad \text{and} \qquad {}^{b}\tilde{\dot{\boldsymbol{r}}}_{\mathrm{s}} = \mathbf{R}_i^b \, {}^{i}\tilde{\dot{\boldsymbol{r}}}_{\mathrm{s}} \tag{4} $$

$$ \mathbf{R}_i^b = \begin{bmatrix} [\boldsymbol{h}/h \times \boldsymbol{r}_{\mathrm{s}}/r]^{\mathsf{T}} \\ \boldsymbol{h}^{\mathsf{T}}/h \\ \boldsymbol{r}_{\mathrm{s}}^{\mathsf{T}}/r \end{bmatrix}, $$

where $\mathbf{R}_i^b$ is the rotation matrix from the the ECI frame $\{i\}$ to the SV's RSW satellite coordinate system $\{b\}$, that is determined using the LEO SV's true dynamic states, where the SV's position vector determines the *radial* axis, the angular momentum vector determines the *cross-track* axis, and finally the common perpendicular to both the radial and cross-track directions determines the *along-track* axis.

Using standard trigonometric identities, the position and velocity errors of the predicted orbit (4) due to an argument-of-latitude error $\tilde{u} \triangleq u - u'$ can be represented in the SV's body frame, i.e., in the along-track (A), cross-track (C), and radial (R) components as

$$ \begin{aligned} {}^{b}\tilde{r}_{\mathrm{s}}{}^{A} &= \frac{r_{\mathrm{s}}}{2(e\cos\nu + 1)} \Big\{ 2\sin\tilde{u} - e[\sin(u' - 2u + \omega) + \sin(u' - \omega)] \Big\} \\ {}^{b}\tilde{r}_{\mathrm{s}}{}^{C} &= 0 \\ {}^{b}\tilde{r}_{\mathrm{s}}{}^{R} &= r_{\mathrm{s}}(1 - \cos\tilde{u}) \end{aligned} \tag{5} $$

$$ \begin{aligned} {}^{b}\tilde{\dot{r}}_{\mathrm{s}}{}^{A} &= \frac{\mu}{2h(e\cos\nu + 1)} \Big\{ -2\cos\tilde{u} + 2 + e[-\cos(u' - 2u + \omega) + 2\cos(u - \omega) - \cos(u' - \omega)] \Big\} \\ {}^{b}\tilde{\dot{r}}_{\mathrm{s}}{}^{C} &= 0 \\ {}^{b}\tilde{\dot{r}}_{\mathrm{s}}{}^{R} &= -\frac{\mu}{h}\sin\tilde{u}. \end{aligned} \tag{6} $$

For perfectly circular orbits, i.e., $e \equiv 0$, the predicted orbit's body frame errors can be further simplified to

$$ \begin{aligned} {}^{b}\tilde{r}_{\mathrm{s}}{}^{A} &= r_{\mathrm{s}}\sin\tilde{u} & \qquad {}^{b}\tilde{\dot{r}}_{\mathrm{s}}{}^{A} &= \frac{\mu}{h}(1 - \cos\tilde{u}) \\ {}^{b}\tilde{r}_{\mathrm{s}}{}^{C} &= 0 & \qquad {}^{b}\tilde{\dot{r}}_{\mathrm{s}}{}^{C} &= 0 \\ {}^{b}\tilde{r}_{\mathrm{s}}{}^{R} &= r_{\mathrm{s}}(1 - \cos\tilde{u}) & \qquad {}^{b}\tilde{\dot{r}}_{\mathrm{s}}{}^{R} &= -\frac{\mu}{h}\sin\tilde{u}. \end{aligned} $$

The following remarks can be deduced from the above expressions. First, the predicted orbit's body frame errors suggest that the along-track position and radial velocity errors are both governed by the $\sin\tilde{u}$ term with different scaling factors and opposite directions. Note that propagation errors are typically concentrated in these two states. Second, the radial position and along-track velocity errors are both governed by the $(1 - \cos\tilde{u})$ term with different scaling factors. Third, a propagation error that is purely concentrated in the argument of latitude element exhibits neither position nor velocity errors in the cross-track direction.

To analyze and evaluate the derived propagation error expressions, two different ephemeris sets for the same LEO SVs were considered: (i) SpaceX-published ephemeris files (SpaceX, 2024) as the true ephemeris and (ii) SGP4-propagated TLE files as the predicted ephemeris. Empirical SV position and velocity errors between the true and predicted ephemeris sets were computed and resolved in the SV's body frame according to (4). On the other hand, the analytical SV position and velocity errors were computed based on the derived expressions in (5) and (6). Fig. 2 shows the error time series over a 1.5-hour duration for four Starlink LEO SVs, labeled by their NORAD IDs. The close match between the empirical and analytical curves shows how the position and velocity errors can be parameterized by the argument of latitude error. It is important to note that the presented analytical expressions do not consider the errors in the remaining orbital elements, namely the angular momentum magnitude, eccentricity, inclination, and right ascension, leading to slight discrepancies with the error values obtained from the ephemerides sets, as seen in Fig. 2.

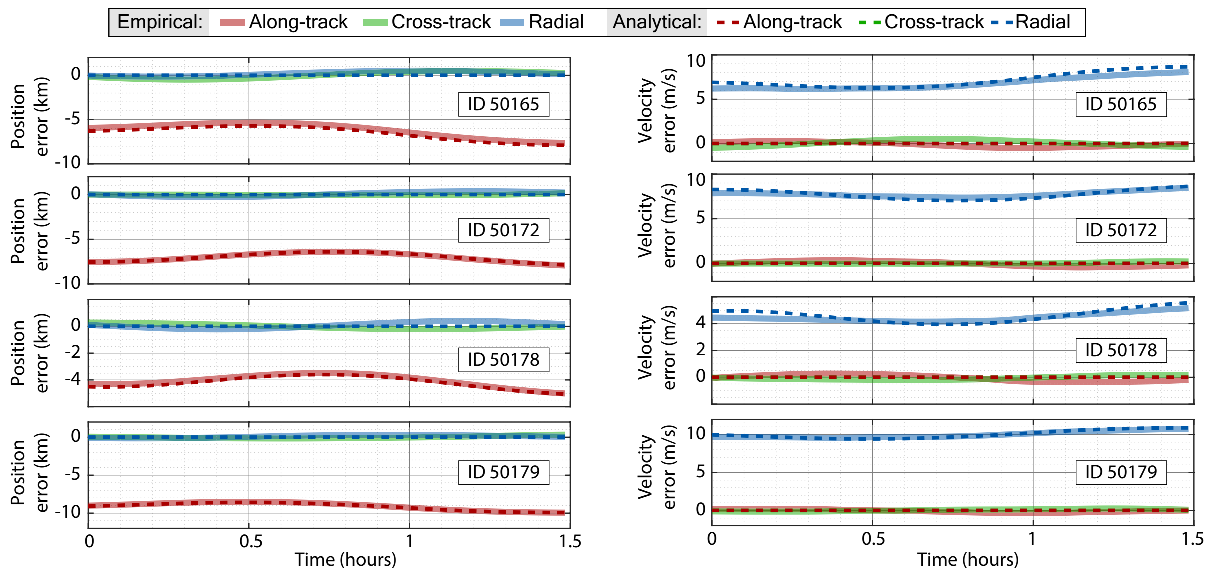

Figure 2: Empirical and analytical SV position (left) and velocity (right) errors in the SV's body frame for 4 Starlink LEO SVs.

3. Ephemeris Epoch Time Adjustment

The SV position and velocity prediction error magnitudes are determined by

$$\tilde{r}_s(t) \triangleq \|\boldsymbol{r}_s(t) - \boldsymbol{r}'_s(t)\|_2, \quad (7)$$
$$\tilde{\dot{r}}_s(t) \triangleq \|\dot{\boldsymbol{r}}_s(t) - \dot{\boldsymbol{r}}'_s(t)\|_2. \quad (8)$$

Using (2) and (3) and standard trigonometric identities, (7) and (8) can be simplified to

$$\tilde{r}_s(t) \approx r_s(t)\sqrt{2(1-\cos[\tilde{u}(t)])}\,, \quad (9)$$
$$\tilde{\dot{r}}_s(t) \approx \frac{\mu}{h(t)}\sqrt{2(1-\cos[\tilde{u}(t)])}\,. \quad (10)$$

The SV position and velocity error magnitudes can be significantly reduced by invoking an epoch time adjustment to the predicted ephemeris. The following analysis explains this phenomenon. The position and velocity errors between the true SV and an epoch time-adjusted version of the predicted SV are written as

$$\tilde{r}_s(t,\tau) \triangleq \|\boldsymbol{r}_s(t) - \boldsymbol{r}'_s(t+\tau)\|, \quad (11)$$
$$\tilde{\dot{r}}_s(t,\tau) \triangleq \|\dot{\boldsymbol{r}}_s(t) - \dot{\boldsymbol{r}}'_s(t+\tau)\|. \quad (12)$$

Using (9) and (10), (11) and (12) can respectively be written as

$$\tilde{r}_s(t,\tau) \approx r_s(t)\sqrt{2(1-\cos[u(t)-u'(t+\tau)])}, \quad (13)$$
$$\tilde{\dot{r}}_s(t,\tau) \approx \frac{\mu}{h(t)}\sqrt{2(1-\cos[u(t)-u'(t+\tau)])}. \quad (14)$$

Using the argument of latitude dynamics described in (1), where the first term is more dominant than the J_2 perturbation term, the following relationship can be established

$$u(t+\tau) \approx u(t) + \frac{h}{r_{\mathrm{s}}^2}\,\tau. \tag{15}$$

Substituting (15) into (13) and (14), the position and velocity errors in terms of the epoch time adjustment become

$$\tilde{r}_{\mathrm{s}}(t,\tau) = r_{\mathrm{s}}(t)\sqrt{2\left(1-\cos\left[\tilde{u}(t)-\frac{\tau h(t)}{r_{\mathrm{s}}^2(t)}\right]\right)}, \tag{16}$$

$$\tilde{\dot{r}}_{\mathrm{s}}(t,\tau) = \frac{\mu}{h(t)}\sqrt{2\left(1-\cos\left[\tilde{u}(t)-\frac{\tau h(t)}{r_{\mathrm{s}}^2(t)}\right]\right)}. \tag{17}$$

The epoch time adjustment that minimizes the position and velocity errors is calculated as

$$\tau^*(t) = \arg\min_{\tau}\ \tilde{r}_{\mathrm{s}}(t,\tau) = \arg\min_{\tau}\ \tilde{\dot{r}}_{\mathrm{s}}(t,\tau) = \frac{r_{\mathrm{s}}^2(t)\tilde{u}(t)}{h(t)}. \tag{18}$$

Moreover, by taking the second derivative of the squared position error with respect to the epoch time adjustment, the convexity property is shown

$$\frac{\partial^2 \tilde{r}_{\mathrm{s}}^2(t,\tau)}{\partial \tau^2} = 2\cos\left(\tilde{u}(t)-\frac{\tau h}{r_{\mathrm{s}}^2}\right)\frac{h^2}{r_{\mathrm{s}}^2} \geq 0, \qquad \text{for } \left|\tilde{u}(t)-\frac{h\tau}{r_{\mathrm{s}}^2}\right| \leq \frac{\pi}{2}, \tag{19}$$

where τ will practically lie in the domain of convexity in (19) since $\tilde{u}$ is much smaller than $\frac{\pi}{2}$.

The effect of ephemeris epoch time adjustment is analyzed by comparing the TLE-initialized, SGP4-propagated position and velocity with real GPS-derived position and velocity data, which is transmitted from Orbcomm satellite-mounted GPS receivers. The truth ephemeris was obtained by a LEO receiver based in Irvine, California, USA, which decoded the transmitted ephemeris from Orbcomm FM107 SV's downlink signals over approximately 280 seconds. Fig. 3 shows the position and velocity errors between the true ephemeris and the SGP4-propagated counterpart, i.e., the plots depict $\tilde{r}_{\mathrm{s}}(t_0,\tau)$ and $\tilde{\dot{r}}_{\mathrm{s}}(t_0,\tau)$ as a function of τ at an arbitrarily chosen fixed time instant $t_0 \equiv 100$ s into the recorded data. The empirical position and velocity errors are calculated according to (11) and (12), respectively, while the analytical position and velocity errors are calculated according to (16) and (17), respectively. The epoch time adjustment that minimizes the position and velocity was obtained empirically at a 1 ms step size and was found to be -949 ms and -917, respectively. On the other hand, the analytical minimizing epoch time adjustment was computed according to (18) and was found to be -996 ms. The discrepancies between the empirical and analytical errors arise due to the assumption that the predicted orbit errors are only translated in an argument of latitude error and do not affect the remaining orbital elements.

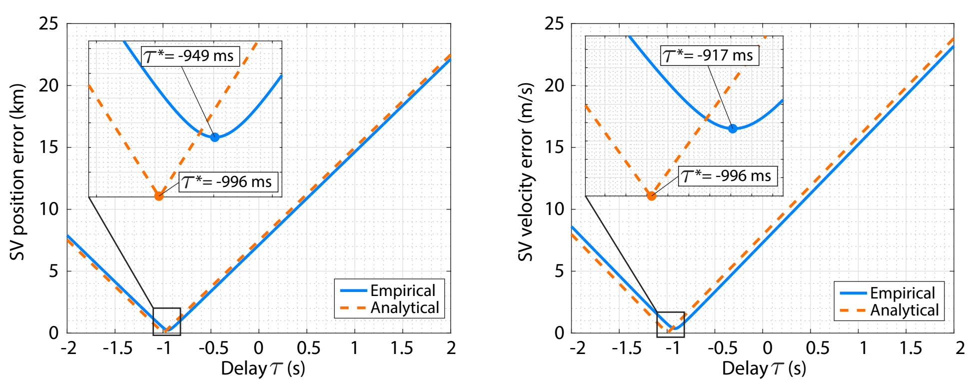

Figure 3: Empirical and analytical SV position (left) and velocity (right) errors versus ephemeris epoch time adjustment τ. The values of τ^* denote the epoch time adjustment that minimizes the SV position and velocity errors, determined empirically or analytically.

To demonstrate the effect of epoch time adjustment on propagated orbit errors, (18) is used to generate an adjusted ephemeris set from the SGP4-propagated ephemeris, denoted $\{\boldsymbol{r}'(t+\tau^*(t))\,,\ \dot{\boldsymbol{r}}'(t+\tau^*(t))\}$. Fig. 4 shows (top) the original SGP4 position and velocity errors, computed as $\|\boldsymbol{r}_{\mathrm{s}}(t)-\boldsymbol{r}'_{\mathrm{s}}(t)\|_2$ and $\|\dot{\boldsymbol{r}}_{\mathrm{s}}(t)-\dot{\boldsymbol{r}}'_{\mathrm{s}}(t)\|_2$, respectively, and (bottom) the epoch time-adjusted SGP4 position and velocity errors, computed as $\|\boldsymbol{r}_{\mathrm{s}}(t)-\boldsymbol{r}'_{\mathrm{s}}(t+\tau^*(t))\|_2$ and $\|\dot{\boldsymbol{r}}_{\mathrm{s}}(t)-\dot{\boldsymbol{r}}'_{\mathrm{s}}(t+\tau^*(t))\|_2$, respectively. The

RMSE of the SGP4-propagated position and velocity decreased from about 7,136 m to 392 m and from about 7.39 m/s 0.67 m/s after the epoch time adjustment. This experimental analysis shows the significant improvement in the accuracy of the epoch time-adjusted predicted orbit. Note that the remaining errors are due to the aforementioned assumptions in the computation of $\tau^*(t)$ as well as the original cross-track and radial errors in the predicted orbit.

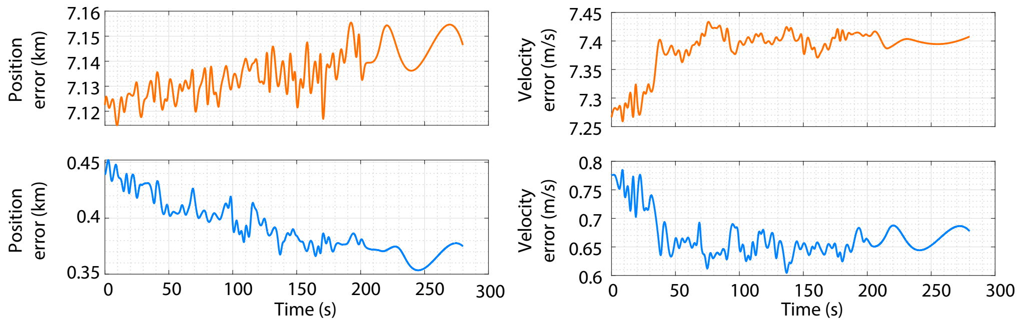

Figure 4: Orbcomm FM107 position and velocity errors before (top) and after (bottom) epoch time adjustment.

Ephemeris epoch time adjustment was also analyzed with SpaceX published accurate ephemerides files (SpaceX, 2024), considered as the true orbit versus TLE-initialized SGP4-propagated ephemerides, considered as the predicted orbit. Fig. 5(a) shows the calculated epoch time adjustment according to (18) for four Starlink LEO SVs, labeled by their NORAD IDs. Fig. 5(b) and (c) show the original predicted orbit position and velocity errors, while Fig. 5(d) and (e) show the the epoch time-adjusted SGP4 position and velocity errors, computed as $\|\boldsymbol{r}_\text{s}(t) - \boldsymbol{r}'_\text{s}(t + \tau^*(t))\|_2$ and $\|\dot{\boldsymbol{r}}_\text{s}(t) - \dot{\boldsymbol{r}}'_\text{s}(t + \tau^*(t))\|_2$, respectively. The errors decreased by approximately one order of magnitude after the epoch time adjustment.

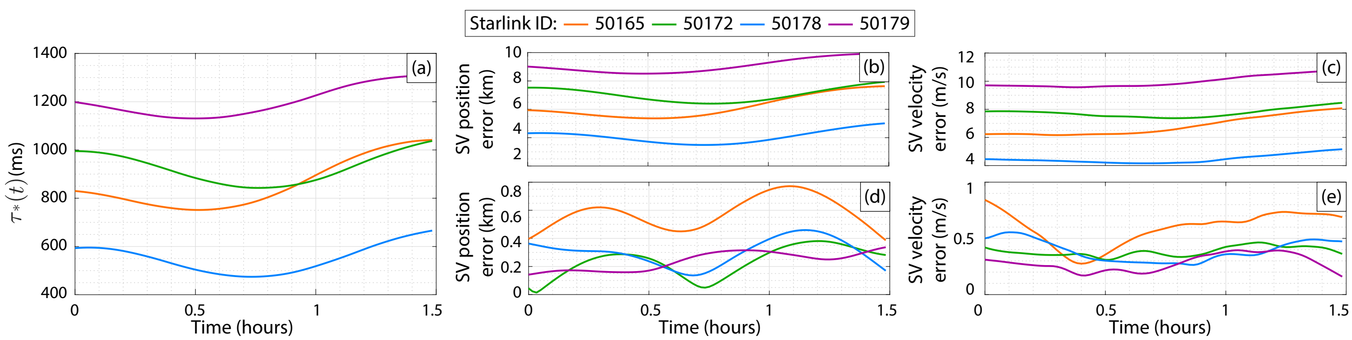

Figure 5: (a) Epoch time adjustment calculated according to (18) for four different Starlink SVs. SV (b) position and (c) velocity errors of the original open-loop SGP4-propagated orbits. SV (d) position and (e) velocity errors of the epoch time adjusted SGP4-propagated orbits.

III. EXPERIMENTAL RESULTS

This section presents UAV navigation experimental results validating the proposed ephemeris error correction with Orbcomm LEO SV signals. The experimental setup is first described and then experimental results are presented.

1. Experimental Setup

A DJI Matrice 600 UAV was equipped with an Ettus E312 universal software radio peripheral (USRP), a high-end very high frequency (VHF) antenna, and a small consumer-grade GPS antenna to discipline the onboard oscillator. The receiver was tuned to a 137 MHz carrier frequency with 2.4 Msps sampling bandwidth to collect downlink Orbcomm signals that are transmitted in the 137-138 MHz band. Samples of the received signals were stored for off-line post-processing. The software defined radio (SDR) implementation discussed in (Kozhaya and Kassas, 2022) was used to generate carrier phase measurements from the collected samples. The ground truth UAV trajectory was taken from its GNSS-based on-board navigation system. The experimental hardware setup is shown in Fig. 6(a). The UAV traversed a total trajectory of 780 m in 90 seconds. Over the course of the trajectory, the on-board receiver collected signals from 2 Orbcomm LEO SVs, namely FM108 and FM116. A skyplot of the 2 Orbcomm SVs is shown in Fig. 6(b), demonstrating the relative geometries of the SVs with respect to the UAV. The carrier phase measured by the receiver for the 2 Orbcomm SVs is shown along with the expected carrier phase calculated from TLE files and SGP4 software in Fig. 6(c).

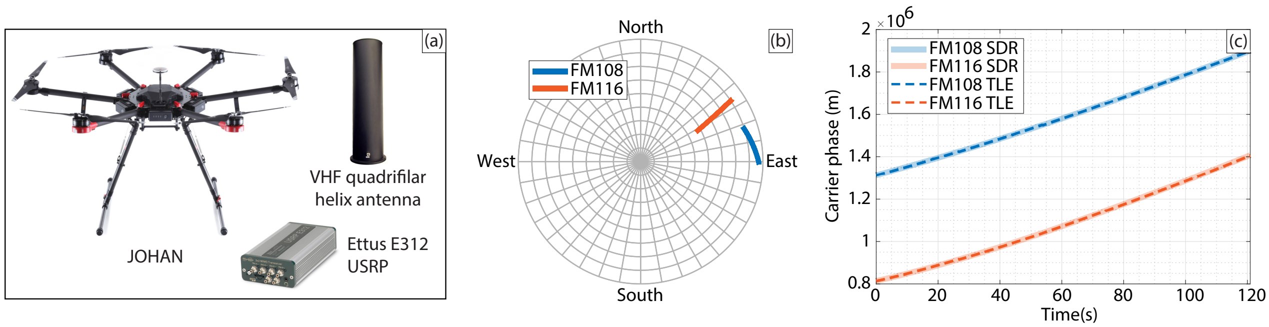

Figure 6: Experimental setup and environment: (a) UAV on-board signal collection hardware, (b) skyplot of the 2 Orbcomm SVs during the experiment, and (c) the measured carrier phase using the SDR and the expected carrier phase based on the TLE for both Orbcomm SVs.

2. Navigation Filter Settings

GNSS measurements were only available to the UAV during the first 30 seconds of the flight duration, during which the ephemeris correction approach discussed in Section II was implemented, before being virtually cut off for the remaining 60 seconds, during which the UAV navigated with LEO signals. The argument of latitude errors were estimated via a batch least squares that incorporated the first 30 seconds of carrier measurements to the 2 LEO SVs (Hayek and Kassas, 2024). Next, the epoch time adjustment was computed based on (18) and was found to be $\tau_1^* = 190.8$ms and $\tau_2^* = 14.6$ms for Orbcomm FM108 and FM116, respectively. These values were applied to the open-loop SGP4-propagated ephemeris for each SV to generate the corrected ephemerides denoted by $\{\boldsymbol{r}'(t+\tau_i^*)\ ,\ \dot{\boldsymbol{r}}'(t+\tau_i^*)\}_{i=1}^2$.

The estimated state vector by the extended Kalman filter (EKF) consisted of the UAV's position and velocity, along with two clock error states, capturing the difference between the receiver's and each LEO SV's clock error states. The UAV's position and velocity were modeled according to a nearly constant velocity model and the clock states were modeled according to the standard double integrator driven by noise (Brown and Hwang, 1997). Note that the carrier phase ambiguity term λN was lumped into the clock error states for each SV. The UAV's continuous-time acceleration process noise spectra were set to $\tilde{q}_{\text{E}} = \tilde{q}_{\text{N}} = 5\ \text{m}^2/\text{s}^3$ and $\tilde{q}_{\text{U}} = 0.05\ \text{m}^2/\text{s}^3$ for the East, North, and Up components, respectively. The choice of these spectra is due to the fact that the UAV's maneuvers are mainly in the horizontal direction. The position and velocity process noise covariance matrix can be readily obtained from these power spectra (Kassas and Humphreys, 2014). The UAV's and LEO SV's oscillator qualities were both assumed to be that of a typical oven-controlled crystal oscillator (OCXO), from which the process noise covariance can also be readily obtained (Kassas and Humphreys, 2014). A prior for the UAV position and velocity was obtained from the UAV's on-board GNSS system. The initial UAV position and velocity estimation error covariance values were set to $\mathbf{P}_{\boldsymbol{r}_r}(0|0) \equiv 10 \cdot \mathbf{I}_{3\times3}\ \text{m}^2$ and $\mathbf{P}_{\dot{\boldsymbol{r}}_r}(0|0) \equiv \mathbf{I}_{3\times3}$ (m/s)^2, respectively. The initial estimation error covariance for the clock error states of each SV was set to $\mathbf{P}_{\text{clk}}(0|0) \equiv \text{diag}[9\times10^4, 9\times10^2]$ with units $[\text{m}^2, (\text{m/s})^2]$, corresponding to a 1σ of 1 μs and 0.1 μs/s for the clock bias and drift, respectively. The carrier phase measurement noise was modeled as a discrete-time zero-mean white Gaussian sequence with variance σ_i^2. The filter's time-varying measurement noise standard deviations were set to be equal to the measurement innovations for each SV and ranged between 0.85 mm and 15.08 m for Orbcomm FM108 and 2.90 mm and 16.94 m for Orbcomm FM116. Altimeter measurements from the UAV's on-board navigation system were also fused into the EKF with a noise variance of 3 m^2. To demonstrate the benefit of correcting the LEO SV ephemerides, the UAV's 3-D position was estimated using the carrier phase measurements from the 2 LEO SVs using (i) the open-loop SGP4-propagated versus (ii) the corrected ephemerides.

3. Results

The navigation results demonstrate the advantages of adopting the ephemerides correction strategy. Fig. 7 shows the EKF UAV position and velocity estimation errors along with the $\pm3\sigma$ uncertainty bounds for the open-loop SGP4 ephemerides case. The errors are resolved in the local navigation frame, namely the East, North, and Up directions. The UAV position estimate is inconsistent as the error is not contained within the uncertainty bounds. This is due to the model mismatch in the filter when using the open-loop SGP4-propagated ephemerides that suffer from SV position errors. Fig. 8 shows the EKF UAV position and velocity estimation errors along with the $\pm3\sigma$ uncertainty bounds for the corrected ephemerides case. The errors are bounded by the filter's uncertainty which is slightly diverging during the flight duration. This divergence could be attributed to stochastic observability issues (Mortlock and Kassas, 2020). The altitude measurements prevent the divergence of the Up direction errors in both cases. The 3D position RMSEs and final errors for both cases are summarized in Table 1. The LEO SVs' trajectories are shown in Fig. 9(a) and the UAV ground truth and estimated trajectories are shown in Fig. 9(b).

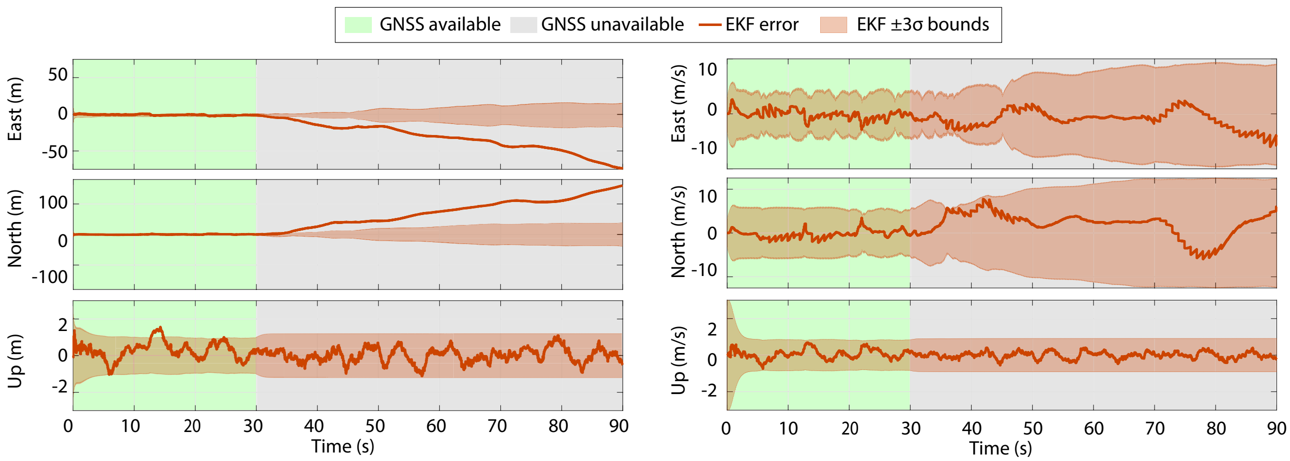

Figure 7: UAV position (left) and velocity (right) EKF estimation errors and $\pm 3\sigma$ bounds, resolved in the ENU frame, where the SV positions are obtained from open-loop SGP4 propagation.

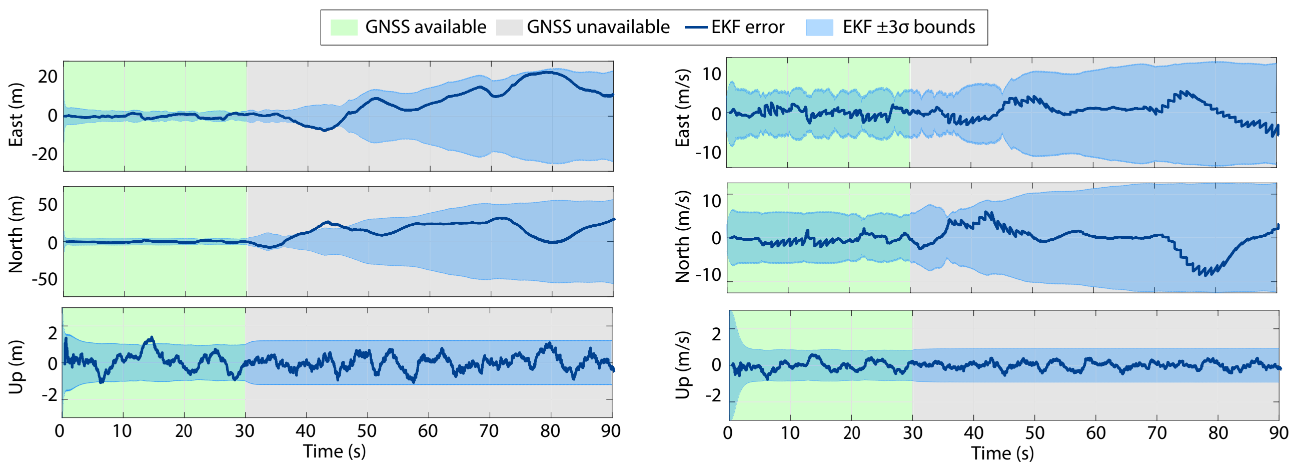

Figure 8: UAV position (left) and velocity (right) EKF estimation errors and $\pm 3\sigma$ bounds, resolved in the ENU frame, where the SV positions are obtained from the corrected ephemerides.

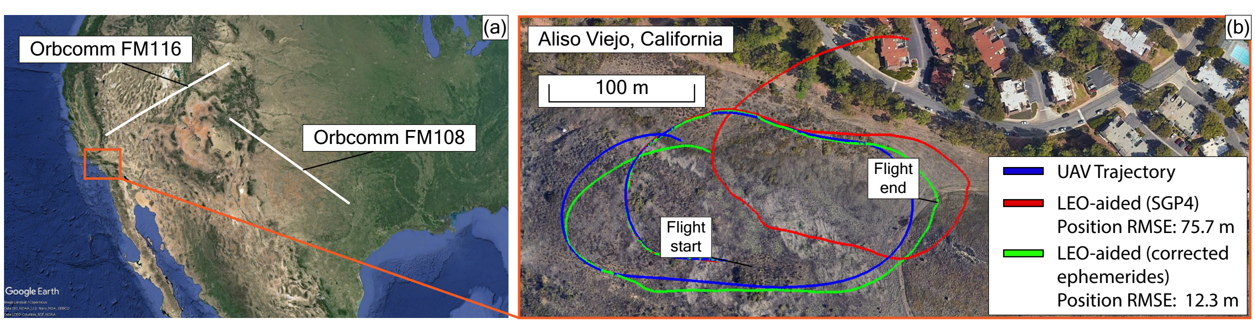

Figure 9: Experimental results: (a) trajectories of the 2 Orbcomm LEO SVs and (b) the UAV's true trajectory and estimated trajectory with (i) open-loop SGP4 propagated and (ii) corrected ephemerides.

Table 1: Experimental results: UAV 3D position RMSEs and 3D final errors

	Position RMSE [m]	**Final error [m]**
Open-loop SGP4 ephemerides	75.69	176.59
Corrected ephemerides	12.28	22.26

IV. CONCLUSION

This paper developed analytical models for LEO SV orbit propagation errors to correct publicly available ephemeris information. The effect of epoch time adjustment was examined and was shown to lead to significant ephemeris error reductions with Orbcomm experimental data as well as SpaceX published accurate ephemerides sets. The advantages of corrected LEO SV ephemerides sets were demonstrated experimentally with UAV opportunistically navigating with carrier phase observables from 2 Orbcomm LEO SVs. It is shown that using open-loop SGP4-propagated ephemerides yields a 3D UAV position RMSE of 75.69 m over a trajectory of 780 m, while incorporating the corrected ephemerides sets resulted in an RMSE of 12.28 m.

ACKNOWLEDGMENTS

The authors would like to thank Sharbel Kozhaya, Joe Khalife, and Joshua Morales for their help in experimental data collection and processing. This work was supported in part by the Air Force Office of Scientific Research (AFOSR) under Grant FA9550-22-1-0476, in part by the National Science Foundation (NSF) under Grant 2240512, and in part by The Aerospace Corporation under Award 4400000428.

REFERENCES

Ardito, C., Morales, J., Khalife, J., Abdallah, A., and Kassas, Z. (2019). Performance evaluation of navigation using LEO satellite signals with periodically transmitted satellite positions. In *Proceedings of ION International Technical Meeting Conference*, pages 306–318.

Brown, R. and Hwang, P. (1997). *Introduction to Random Signals and Applied Kalman Filtering*. John Wiley & Sons, third edition.

Burbank, J., Greene, T., and Kaabouch, N. (2024). Detecting and mitigating attacks on GPS devices. *Sensors*, 24(17):1–47.

Celikbilek, K., Saleem, Z., Morales Ferre, R., Praks, J., and Lohan, E. (2022). Survey on optimization methods for LEO-satellite-based networks with applications in future autonomous transportation. *Sensors*, 22(4):1–52.

Coffee, B., Bishop, R., and Cahoy, K. (2013). Propagation of cubesats in LEO using NORAD two line element sets: Accuracy and update frequency. In *Proceedings of AIAA Guidance, Navigation, and Control Conference*, pages 1–15.

Curtis, H. (2019). *Orbital mechanics for engineering students*. Butterworth-Heinemann, fourth edition.

Easthope, P. (2015). Examination of SGP4 along-track errors for initially circular orbits. *IMA Journal of Applied Mathematics*, 80(2):554–568.

Egea-Roca, D., Lopez-Salcedo, J., Seco-Granados, G., and Falletti, E. (2022). Performance analysis of a multi-slope chirp spread spectrum signal for PNT in a LEO constellation. In *Proceedings of Workshop on Satellite Navigation Technology*, pages 1–9.

Farhangian, F. and Landry, R. (2023). High-order pseudorange rate measurement model for multi-constellation LEO/INS integration: Case of Iridium-NEXT, Orbcomm, and Globalstar. *Proceedings of the Institution of Mechanical Engineers, Part G: Journal of Aerospace Engineering*, 237(4):925–939.

Ferre, R., Praks, J., Seco-Granados, G., and Lohan, E. (2022). A feasibility study for signal-in-space design for leo-pnt solutions with miniaturized satellites. *IEEE Journal on Miniaturization for Air and Space Systems*, 3(4):171–183.

Grayver, E., Nelson, R., McDonald, E., Sorensen, E., and Romano, S. (2024). Position and navigation using Starlink. In *Proceedings of IEEE Aerospace Conference*, pages 1–12.

Hayek, S. and Kassas, Z. (2024). Modeling and compensation of timing and spatial ephemeris errors of non-cooperative leo satellites with application to pnt. *IEEE Transactions on Aerospace and Electronic Systems*. submitted.

Hayek, S., Saroufim, J., and Kassas, Z. (2023). Ephemeris error modeling in opportunistic LEO satellite tracking with pseudorange and Doppler measurements. In *Proceedings of ION GNSS+ Conference*, pages 2123–2133.

Hayek, S., Saroufim, J., and Kassas, Z. (2024). Ephemeris error correction for tracking non-cooperative LEO satellites with pseudorange measurements. In *Proceedings of IEEE Aerospace Conference*, pages 1–9.

Hegarty, C., Bobyn, D., Grabowski, J., and Van Dierendonck, A. (2020). An overview of the effects of out-of-band interference on GNSS receivers. *NAVIGATION, Journal of the Institute of Navigation*, 67(1):143–161.

Huang, C., Qin, H., Zhao, C., and Liang, H. (2022). Phase - time method: Accurate Doppler measurement for Iridium NEXT signals. *IEEE Transactions on Aerospace and Electronic Systems*, 58(6):5954–5962.

Ioannides, R., Pany, T., and Gibbons, G. (2016). Known vulnerabilities of global navigation satellite systems, status, and potential mitigation techniques. *Proceedings of the IEEE*, 104(6):1174–1194.

Jardak, N. and Jault, Q. (2022). The potential of LEO satellite-based opportunistic navigation for high dynamic applications. *Sensors*, 22(7):2541–2565.

Jiang, M., Qin, H., Su, Y., Li, F., and Mao, J. (2023). A design of differential-low Earth orbit opportunistically enhanced GNSS (D-LoeGNSS) navigation framework. *Remote Sensing*, 15(8):2136–2158.

Kang, J., Eberechukwu N, P., Lee, J., Wymeersch, H., and Kim, S. S. (2024). Fundamental performance bounds for carrier phase positioning in LEO-PNT systems. In *Proceedings of IEEE International Conference on Acoustics, Speech and Signal Processing*, pages 13496–13500.

Kassas, Z. and Humphreys, T. (2014). Observability analysis of collaborative opportunistic navigation with pseudorange measurements. *IEEE Transactions on Intelligent Transportation Systems*, 15(1):260–273.

Kassas, Z., Khairallah, N., and Kozhaya, S. (2024). Ad astra: Simultaneous tracking and navigation with megaconstellation LEO satellites. *IEEE Aerospace and Electronic Systems Magazine*, 39(9):46–71.

Kassas, Z., Kozhaya, S., Kanj, H., Saroufim, J., Hayek, S., Neinavaie, M., Khairallah, N., and Khalife, J. (2023). Navigation with multi-constellation LEO satellite signals of opportunity: Starlink, Oneweb, Orbcomm, and Iridium. In *Proceedings of IEEE/ION Position, Location, and Navigation Symposium*, pages 338–343.

Kassas, Z., Morales, J., and Khalife, J. (2019). New-age satellite-based navigation – STAN: simultaneous tracking and navigation with LEO satellite signals. *Inside GNSS Magazine*, 14(4):56–65.

Kelso, T. (2007). Validation of SGP4 and IS-GPS-200D against GPS precision ephemerides. In *Proceedings of AAS/AIAA Space Flight Mechanics Conference*, pages 1–14.

Kelso, T. (2022). NORAD two-line element set format. `https://celestrak.org/NORAD/documentation/tle-fmt.php`.

Khalife, J. and Kassas, Z. (2019). Receiver design for Doppler positioning with LEO satellites. In *Proceedings of IEEE International Conference on Acoustics, Speech and Signal Processing*, pages 5506–5510.

Khalife, J. and Kassas, Z. (2023). Performance-driven design of carrier phase differential navigation frameworks with mega-constellation LEO satellites. *IEEE Transactions on Aerospace and Electronic Systems*, 59(3):2947–2966.

Khalife, J., Neinavaie, M., and Kassas, Z. (2021). Blind Doppler tracking from OFDM signals transmitted by broadband LEO satellites. In *Proceedings of IEEE Vehicular Technology Conference*, pages 1–5.

Khalife, J., Neinavaie, M., and Kassas, Z. (2022). The first carrier phase tracking and positioning results with Starlink LEO satellite signals. *IEEE Transactions on Aerospace and Electronic Systems*, 56(2):1487–1491.

Kozhaya, S., Kanj, H., and Kassas, Z. (2023). Multi-constellation blind beacon estimation, Doppler tracking, and opportunistic positioning with OneWeb, Starlink, Iridium NEXT, and Orbcomm LEO satellites. In *Proceedings of IEEE/ION Position, Location, and Navigation Symposium*, pages 1184–1195.

Kozhaya, S. and Kassas, Z. (2022). Blind receiver for LEO beacon estimation with application to UAV carrier phase differential navigation. In *Proceedings of ION GNSS Conference*, pages 2385–2397.

Kozhaya, S. and Kassas, Z. (2023). Positioning with Starlink LEO satellites: A blind Doppler spectral approach. In *Proceedings of IEEE Vehicular Technology Conference*, pages 1–5.

Landry, R., Nguyen, A., Rasaee, H., Amrhar, A., Fang, X., and Benzerrouk, H. (2019). Iridium Next LEO satellites as an alternative PNT in GNSS denied environments–part 1. *Inside GNSS Magazine*, 14(3):56–64.

Liang, H., Qin, H., and Li, H. (2024). Doppler compensated pseudorange based signal-of-opportunity positioning using Iridium satellite. *IEEE Transactions on Aerospace and Electronic Systems*, pages 1–14.

Liu, P., Voon Ling, K., Qin, H., Jiang, M., and Lu, J. (2024). Actualization analysis of LEO opportunistic doppler aided GNSS precise point positioning using moving horizon estimation. *IEEE Transactions on Vehicular Technology*, pages 1–12. accepted.

Menzione, F. and Paonni, M. (2023). LEO-PNT mega-constellations: a new design driver for the next generation MEO GNSS space service volume and spaceborne receivers. In *Proceedings of IEEE/ION Position, Location, and Navigation Symposium*, pages 1196–1207.

Montenbruck, O. and Gill, E. (2000). *Satellite orbits: models, methods, and applications*. Springer.

Morales, J., Khalife, J., Abdallah, A., Ardito, C., and Kassas, Z. (2018). Inertial navigation system aiding with Orbcomm LEO satellite Doppler measurements. In *Proceedings of ION GNSS Conference*, pages 2718–2725.

Mortlock, T. and Kassas, Z. (2020). Performance analysis of simultaneous tracking and navigation with LEO satellites. In *Proceedings of ION GNSS Conference*, pages 2416–2429.

Osoro, O. and Oughton, E. (2021). A techno-economic framework for satellite networks applied to low earth orbit constellations: Assessing Starlink, Oneweb and Kuiper. *IEEE Access*, 9:141611–141625.

Prol, F., Bhuiyan, M., Kaasalainen, S., Lohan, S., Praks, J., Celikbilek, K., and Kuusniemi, H. (2024). Simulations of dedicated LEO-PNT systems for precise point positioning: Methodology, parameter analysis, and accuracy evaluation. *IEEE Transactions on Aerospace and Electronic Systems*, pages 1–19. accepted.

Prol, F., Ferre, R., Saleem, Z., Välisuo, P., Pinell, C., Lohan, E., Elsanhoury, M., Elmusrati, M., Islam, S., Celikbilek, K., Selvan, K., Yliaho, J., Rutledge, K., Ojala, A., Ferranti, L., Praks, J., Bhuiyan, M., Kaasalainen, S., and Kuusniemi, H. (2022). Position, navigation, and timing (PNT) through low earth orbit (LEO) satellites: A survey on current status, challenges, and opportunities. *IEEE Access*, 10:83971–84002.

Reid, T., Chan, B., Goel, A., Gunning, K., Manning, B., Martin, J., Neish, A., Perkins, A., and Tarantino, P. (2020). Satellite navigation for the age of autonomy. In *Proceedings of IEEE/ION Position, Location and Navigation Symposium*, pages 342–352.

Ries, L., Limon, M., Grec, F., Anghileri, M., Prieto-Cerdeira, R., Abel, F., Miguez, J., Perello-Gisbert, J., d'Addio, S., R. Ioannidis and, A. O., Rapisarda, M., Sarnadas, R., and Testani, P. (2023). LEO-PNT for augmenting Europe's space-based PNT capabilities. In *Proceedings of IEEE/ION Position, Location, and Navigation Symposium*, pages 329–337.

Riesing, K. (2015). Two line element sets of cubesats in LEO: Accuracy assessment and estimation techniques for improvement. In *Proceedings of Annual AIAA/USU Conference on Small Satellites*, pages 1–8.

Saroufim, J., Hayek, S., and Kassas, Z. (2023). Simultaneous LEO satellite tracking and differential LEO-aided IMU navigation. In *Proceedings of IEEE/ION Position Location and Navigation Symposium*, pages 179–188.

Shahcheraghi, S. and Kassas, Z. (2024). A computationally efficient approach for acquisition and Doppler tracking for PNT with LEO megaconstellations. *IEEE Signal Processing Letters*, 31:2400–2404.

Shi, C., Zhang, Y., and Li, Z. (2023). Revisiting Doppler positioning performance with LEO satellites. *GPS Solutions*, 27(3):126–137.

Shuster, S. (2017). A survey and performance analysis of orbit propagators for LEO, GEO, and highly elliptical orbits. Master's thesis, Utah State University, Utah, USA.

Singh, U., Shankar, M., and Ottersten, B. (2022). Opportunistic localization using LEO signals. In *Proceedings of Asilomar Conference on Signals, Systems, and Computers*, pages 894–899.

SpaceX (2024). Public files. `https://www.space-track.org/#publicFiles`.

Stock, W., Hofmann, C., and Knopp, A. (2023). LEO-PNT with Starlink: Development of a burst detection algorithm based on signal measurements. In *Proceedings of International ITG Workshop on Smart Antennas and Conference on Systems, Communications, and Coding*, pages 1–6.

Stock, W., Schwarz, R., Hofmann, C., and Knopp, A. (2024). Survey on opportunistic PNT with signals from LEO communication satellites. *IEEE Communications Surveys & Tutorials*, pages 1–31. accepted.

Vallado, D. and Crawford, P. (2008). SGP4 orbit determination. In *Proceedings of AIAA/AAS Astrodynamics Specialist Conference and Exhibit*, pages 6770–6799.

Yan, T., Wang, Y., Li, T., Tian, Y., Qu, B., and Bian, L. (2023). MCSK signal for LEO satellite constellation based navigation augmentation system. In *Proceedings of China Satellite Navigation Conference*, pages 295–304.

Yang, C., Zang, B., Gu, B., Zhang, L., Dai, C., Long, L., Zhang, Z., Ding, L., and Ji, H. (2023). Doppler positioning of dynamic targets with unknown LEO satellite signals. *Electronics*, 12(11):2392–2404.

Zhao, C., Qin, H., and Li, Z. (2022). Doppler measurements from multiconstellations in opportunistic navigation. *IEEE Transactions on Instrumentation and Measurement*, 71:1–9.

Zhao, C., Qin, H., Wu, N., and Wang, D. (2023). Analysis of baseline impact on differential Doppler positioning and performance improvement method for LEO opportunistic navigation. *IEEE Transactions on Instrumentation and Measurement*, 72:1–10.